Nanotechnology **18** (2007) 305704 (8pp) doi:10.1088/0957-4484/18/30/305704

The coupled effects of geometry and surface orientation on the mechanical properties of metal nanowires

Changjiang Ji and Harold S Park

Department of Civil and Environmental Engineering, Vanderbilt University, Nashville, TN 37235, USA

E-mail: harold.park@vanderbilt.edu

Received 19 April 2007, in final form 21 May 2007
Published 29 June 2007
Online at stacks.iop.org/Nano/18/305704

Abstract
We have performed atomistic simulations of the tensile loading of ⟨100⟩ and ⟨110⟩ copper nanowires to investigate the coupled effects of geometry and surface orientation on their mechanical behaviour and properties. By varying the nanowire cross section from square to rectangular, nanowires with dominant surface facets are created that exhibit distinct mechanical properties due to the different inelastic deformation mechanisms that are activated. In particular, we find that non-square nanowires generally exhibit lower yield stresses and strains, lower toughness, elevated fracture strains, and a propensity to deform via twinning; we quantify the links between the observed deformation mechanisms due to non-square cross section and the resulting mechanical properties, while illustrating that geometry can be utilized to tailor the mechanical properties of nanowires.

1. Introduction

Nanowires have recently been amongst the most studied nanomaterials due to continuous discoveries confirming their superior physical properties compared to larger bulk materials. These physical properties arise in a variety of scientific and engineering disciplines, including optics, magnetism, mechanics, thermal sciences and others [1–5]. These superior physical properties are the reason why nanowires are viewed as being the potential building blocks of future nanoelectromechanical systems (NEMS) [6, 7].

The mechanical properties of metal nanowires have been studied extensively for two major reasons: (1) to gain fundamental information about the strength of nanomaterials, and how free surfaces, which are prevalent in nanomaterials, contribute to the unique properties of nanowires [8–12]; (2) because the physical properties of nanowires are intricately coupled, i.e. electromechanical [13–15] and optomechanical [16–19], it is critical to understand the mechanical properties of deforming nanowires so that highly multifunctional NEMS can be designed.

The current state of understanding on the mechanical behaviour and properties of nanowires has come from both experiment [20–28] and atomistic calculations [29–44]. This collection of information has established that, in general, nanowires have significantly higher yield stresses and strains than bulk materials, that single defects can cause catastrophic losses of strength in single-crystal nanomaterials, and that the mechanical properties are strongly dependent on the axial orientation of the nanowires.

Most simulations of the mechanical behaviour of nanowires have focused on regular geometries (i.e. square cross section) with ⟨100⟩ axial orientations. However, recent experiments have elegantly shown that the geometry of nanomaterials can be controlled through temperature [45, 46], and that geometry can distinctly alter the physical properties of nanomaterials. For example, geometry is known to have a large effect on the optical properties of metal nanoparticles [47]. More recent work has analysed the optical properties of hollow metallic nanostructures [48, 49]; it was found that the optical properties can be altered by hollowing out the nanostructure. While it was recently determined that the transverse surface orientation has a first-order effect on the mechanical behaviour and properties of nanowires, the effects of geometry have, with few exceptions [41, 43, 50], not been analysed.

This paper constitutes a detailed analysis following the earlier work of Ji and Park [50], who found that simply changing the cross-sectional geometry of ⟨100⟩ copper nanowires with {100} surfaces from square to rectangular changed the tensile deformation mode from distributed plasticity via partial dislocation nucleation and propagation to a twinning-dominated deformation mode which allowed the {100} surfaces to reorient to lower-energy {111} surfaces. However, in that work, only ⟨100⟩ nanowires with {100} surfaces were considered; therefore, the generality of the geometric effects on nanowire mechanical properties has not been fully established or investigated.

In this work, we follow through on our earlier work [50] by comprehensively studying the tensile deformation of both ⟨100⟩ and ⟨110⟩ nanowires with various cross-sectional geometries and {100}, {110} and {112} surface orientations. In doing so, we find that, by altering the cross-sectional geometry from square to rectangular, the nanowire deformation modes can change from the slip of full and partial dislocations to organized and diffusionless twinning. Accordingly, the mechanical properties of the nanowires vary greatly depending on the cross-sectional geometry, leading to significant disparities in yield stress and strain, fracture strain and toughness. Because varying the geometry results in creating nanowires with multiple surface facets of different size and orientation, we demonstrate that altering the nanowire cross-sectional geometry creates a coupling between geometry and the exposed transverse surface orientations that dictates the observed deformation modes and mechanical properties of the nanowires.

2. Simulation details

In this work, we performed molecular dynamics simulations on copper nanowires using the embedded atom method (EAM) [51, 52] as the underlying interatomic interaction model. In the EAM, the total energy U for a system of atoms is written as

$$U = \sum_{i}^{N} \left(F_i(\bar{\rho}_i) + \tfrac{1}{2} \sum_{j \neq i}^{N} \phi_{ij}(R_{ij}) \right), \qquad (1)$$

where the summations in (1) extend over the total number of atoms N in the system, F_i is the embedding function, $\bar{\rho}_i$ is the electron density at atom i, ϕ_{ij} is a pair interaction function and R_{ij} is the distance between atoms i and j. In this work, we utilize the EAM potential developed by Mishin *et al* [53], which accurately represents the elastic properties and surface energies of copper. More importantly, the potential accurately captures the stacking fault and twinning energies, which is critical in analysing inelastic deformation.

The nanowires utilized in this study are categorized into four groups according to their axial and surface orientations, as shown in figure 1. The ⟨100⟩/{100} wire has a ⟨100⟩ axial orientation with four {100} side surfaces, while the ⟨100⟩/{110} wire has the same axial orientation but four {110} side surfaces. The ⟨110⟩/{100}{110} wire has a ⟨110⟩ longitudinal axial orientation with two {100} and two {110} side surfaces, while the ⟨110⟩/{111}{112} wire has two {111} and two {112} side surfaces. Of these nanowires, some have been observed experimentally: ⟨100⟩/{100} wires [26, 54], ⟨100⟩/{110} wires [55], and ⟨110⟩/{100}{110} wires [26, 54]. The ⟨110⟩/{111}{112} wire has not been observed experimentally and is presented here for comparative analysis.

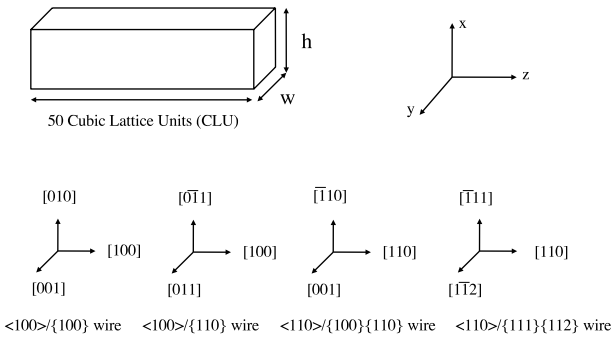

Figure 1. Schematic of the ⟨100⟩ and ⟨110⟩ copper nanowires and the different side surface orientations considered in this work; 1 cubic lattice unit (CLU) = 0.3615 nm for copper.

Table 1. Cross-sectional dimensions in terms of $w \times h$ for ⟨100⟩ copper nanowires, where w and h are defined in figure 1. All dimensions are in CLU.

Orientation	1	2	3	4
⟨100⟩/{100}	5 × 5	5 × 10	5 × 15	5 × 20
⟨100⟩/{110}	5 × 5	5 × 10	5 × 15	5 × 20

The ⟨100⟩ and ⟨110⟩ wires were created by slicing a collection of atoms from a bulk face-centred cubic (fcc) copper crystal. The lengths were all 50 cubic lattice units (CLU) in the z-direction, where 1 CLU = 0.3615 nm for copper, but with different cross-sectional geometries. The various cross-sectional dimensions of the nanowires in terms of $w \times h$ in figure 1 are given in tables 1 and 2. The purpose of varying the cross-sectional dimensions from square to rectangular is to bias one of the surface orientations over the other for a given nanowire, and to observe the effects on the nanowire deformation mechanisms and mechanical properties. For example, for the ⟨110⟩/{100}{110} wires, creating a rectangular cross section would enlarge either the {100} or the {110} surface.

The copper nanowires were first relaxed to energy minimizing positions using the conjugate gradient method; the wires were then equilibrated at 10 K using a Nosé–Hoover thermostat [56, 57] for 100 ps before being loaded in tension along the z-direction. The uniaxial loading was performed by fixing one end of the wire, then applying velocities to atoms along the loading direction that goes linearly from zero at the fixed end to a maximum value at the free end, creating a ramp velocity profile. This ramp velocity was used to avoid the emission of shock waves from the fixed end. Recent work [43] has studied the tensile deformation of metal nanowires using various tensile loading techniques; it was observed that the nanowire deformation mechanisms and mechanical properties are generally independent of the loading mechanism employed.

The loading rate in this work was on the order of $\dot{\epsilon} \approx 10^9$ s^{-1}; this high strain rate compared to those observed experimentally is required to resolve the extremely high vibrational frequency of atoms, which is on the order

Table 2. Cross-sectional dimensions in terms of $w \times h$ for ⟨110⟩ copper nanowires, where w and h are defined in figure 1. All dimensions are in CLU.

Orientation	1	2	3	4	5	6	7
⟨110⟩/{100}{110}	20 × 5	15 × 5	10 × 5	5 × 5	5 × 10	5 × 15	5 × 20
⟨110⟩/{112}{111}	20 × 5	15 × 5	10 × 5	5 × 5	5 × 10	5 × 15	5 × 20

of femtoseconds (10^{-15} s). During the loading process, no thermostat was applied to ensure adiabatic conditions. The equations of motion were integrated in time using a velocity Verlet algorithm, and all simulations were performed using the Sandia-developed code Warp [58, 59]. No periodic boundary conditions were used at any point in the simulations to capture the relevant surface effects.

In this paper, we utilize engineering strain as the measure of deformation; engineering strain is defined as $(l - l_0)/l_0$, where l is the current wire length and l_0 is the initial length of the wire after energy minimization. The stresses were calculated using the virial theorem [60, 61], which takes the form

$$\sigma_{ij} = \frac{1}{V}\left(\frac{1}{2}\sum_{\alpha=1}^{N}\sum_{\beta\neq\alpha}^{N} U'(r^{\alpha\beta})\frac{\Delta x_i^{\alpha\beta}\,\Delta x_j^{\alpha\beta}}{r^{\alpha\beta}} - \sum_{\alpha=1}^{N} m_\alpha \dot{x}_i^\alpha \dot{x}_i^\alpha\right), \tag{2}$$

where N is the total number of atoms, $r^{\alpha\beta}$ is the distance between two atoms α and β, $\Delta x_j^{\alpha\beta} = x_j^\alpha - x_j^\beta$, U is the potential energy, $r^{\alpha\beta} = \|\Delta x_j^{\alpha\beta}\|$, and V is the current volume. The yield strain and yield stress were both found at the point of initial yield, or when the first defect which typically appears in the form of a partial dislocation nucleates within the nanowire. The fracture strain is measured at the breaking point to characterize the capacity of sustaining deformation, while the toughness μ_t is defined as the strain energy density of the nanowire at the fracture point,

$$\mu_t = \int_0^{\epsilon_f} \sigma \, d\epsilon, \tag{3}$$

where ϵ_f is the fracture strain and σ is the uniaxial tensile stress. The unit of toughness is GJ m^{-3} for all the metal nanowires in this paper.

3. Simulation results

3.1. Tension of ⟨100⟩/{100} *and* ⟨100⟩/{110} *nanowires*

We now present our simulation results on the tensile-loaded ⟨100⟩ nanowires; the dimensions considered are given in table 1, while the orientations are shown in figure 1.

The deformation modes of tensile-loaded rectangular ⟨100⟩ nanowires have been evaluated in comparison to square nanowires in previous work by the authors [50]. As illustrated in figure 2, the tensile-loaded square nanowire exhibits yield and plasticity through the nucleation and propagation of full and partial dislocations, while the rectangular wire shows diffusionless and twinning-dominated reorientation in the post-yield deformation period. Specifically, the larger {100} surfaces reorient to form lower-energy {111} surfaces as seen in figure 1(a), while the smaller {100} surfaces reorient to form higher-energy {110} surfaces. Furthermore, the influence of

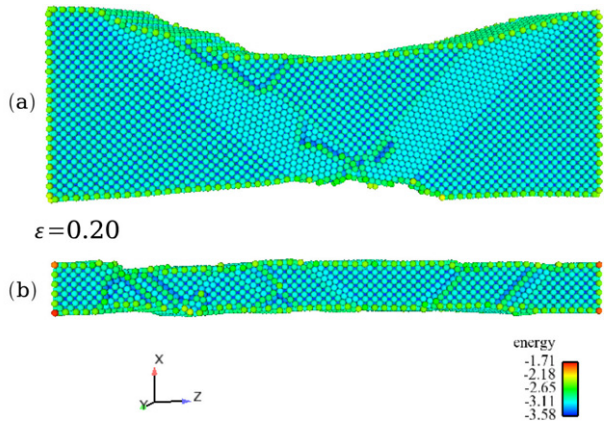

Figure 2. Snapshots of the tensile loaded ⟨100⟩/{100} nanowires at a strain of $\epsilon = 0.20$: (a) 20 × 5 CLU cross section; (b) 5 × 5 CLU cross section. Potential energy is in units of eV.

thickness on the geometry effect has also been considered in that work: thin wires tend to show twin structures due to the strong surface confinement, while thick nanowires are found to deform with full and partial dislocations.

In addition to the influence of wire thickness, the side surface orientation has been found to have a first-order effect on the deformation modes of fcc metal nanowires [40]. In the present work, we wish to investigate the coupled effects of side surface orientation and geometry; therefore, we performed atomistic simulations of the tensile deformation of ⟨100⟩/{110} square and rectangular nanowires. The ⟨100⟩/{110} nanowires have the same axial orientation and cross-sectional sizes as ⟨100⟩/{100} wires, but with the crystal rotated about the ⟨100⟩ axis by 45°, resulting in exposed {110} side surfaces.

Snapshots of the tensile-loaded ⟨100⟩/{110} wires are presented in figure 3. As is shown, the square ⟨100⟩/{110} nanowire accommodates plastic deformation by showing dispersed full and partial dislocations along the axial direction, which is similar to what has been observed in the square ⟨100⟩/{100} wire. In contrast, the rectangular ⟨100⟩/{110} nanowire, instead of deforming via twinning, as observed in rectangular ⟨100⟩/{100} wires, exhibits localized plastic deformation by showing full and partial dislocations. Thus the twinning behaviour observed in rectangular ⟨100⟩/{100} wires resulting from the change in cross-sectional geometry does not apply to ⟨100⟩/{110} wires due to the inability to cause reorientation of the high-energy {110} side surfaces.

The localized plastic deformation observed in ⟨100⟩/{110} nanowires is related to the crystallographic arrangement of the side surfaces. In the rectangular ⟨100⟩/{110} nanowire, the initial stacking fault initiated at the corner of the {100} surface. The stacking fault then moves to the surface and creates a surface step, or full dislocation. The surface step impedes the motion of partial dislocations and their resulting stacking

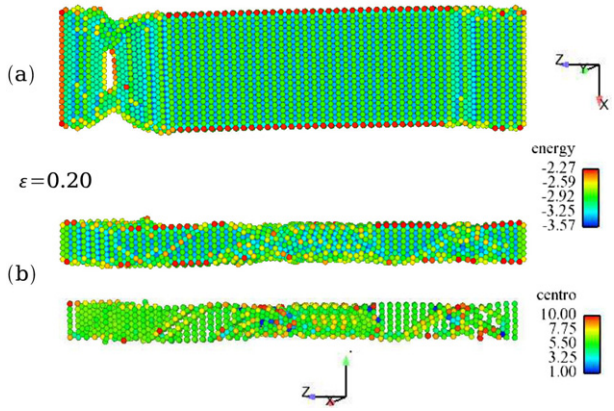

Figure 3. Snapshots of the tensile-loaded ⟨100⟩/{110} nanowires at a strain of $\epsilon = 0.20$: (a) 20 × 5 CLU cross section; (b) 5 × 5 CLU cross section. The top two images show potential energy in units of eV, while the bottom image presents the atomic structure using the centrosymmetry parameter [62].

faults, and thus further deformation is restricted to a small volume around the surface step, leading to the localized fracture observed in figure 3(a).

The stress–strain curves of the tensile-loaded ⟨100⟩ nanowires are presented in figure 4. As is shown, the square ⟨100⟩/{100} nanowire with a 5 × 5 cross section has an extremely large yield stress and strain compared to those of the rectangular ⟨100⟩/{100} nanowire with the 20×5 cross section. As shown in figure 4(a), the 5 × 5 wire yields at 12.6 GPa, while the 20 × 5 yields at 7.2 GPa. This yield stress and strain disparity occurs for two reasons. First, smaller wires tend to relax/contract more due to surface stresses during the initial energy minimization; therefore, they can sustain larger stresses and strains before yielding [38]. We note that recent work has demonstrated that the amount of relaxation that the wires undergo is independent of the ratio of surface area to volume, and instead depends strongly upon the transverse surface area that is exposed by the nanowires [63].

The second, and more important, reason is that different inelastic deformation mechanisms that cause distinct surface reorientations are active for the rectangular ⟨100⟩/{100} nanowires. We note that the rectangular ⟨100⟩/{100} nanowires deform via twinning, which occurs by the nucleation and propagation of successive partial dislocations. In contrast, the full dislocations that are observed in the square ⟨100⟩/{100} nanowires are energetically unfavourable, leading to higher yield stresses in the square ⟨100⟩/{100} nanowires. Furthermore, the rectangular nanowires lower their surface energy as the {100} surfaces reorient to close-packed and thus lower-energy {111} surfaces; the combination of the energetically favourable surface reorientation and the relative ease of nucleating and propagating the twin boundaries result in the dramatically lower yield stress and strain for the rectangular ⟨100⟩/{100} nanowires, as observed in figure 4(a).

After the initial yield, the ⟨100/⟩{100} wires all exhibit a stress plateau of varying length, as shown in figure 4(a). The stress plateau for the 5 × 5 wire extends for about 18% strain, while the stress plateau has a magnitude of nearly 3.5 GPa. In contrast, the stress plateau for the 20 × 5 wire extends for about 26% strain, with a smaller stress magnitude of about

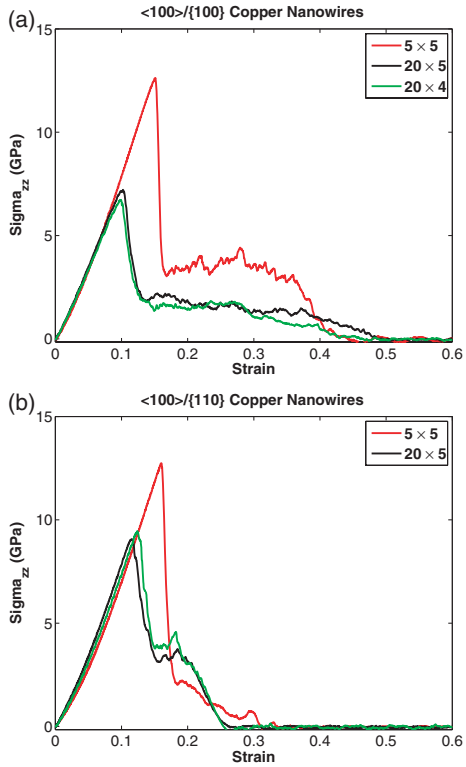

Figure 4. Stress–strain curves of tensile-loaded ⟨100⟩ copper nanowires: (a) ⟨100⟩/{100} wires; (b) ⟨100⟩/{110} wires.

Table 3. The toughness (μ_t) of ⟨100⟩ copper nanowires under tensile loading. The values are in units of GJ m^{-3} and correspond to the wires in table 1.

Orientation	1	2	3	4
⟨100⟩/{100}	1.69	0.90	1.14	0.94
⟨100⟩/{110}	1.12	1.02	0.89	0.92

1.6 GPa. The longer stress plateau leads to a larger post-yield ductility, which results from the twinning-dominated behaviour. The difference in the stress plateau magnitude is rooted in different deformation mechanisms: the larger stress plateau for the square nanowires occurs due to the propagation of higher energy full and partial dislocations and the resulting stacking faults, while the lower stress plateau in the rectangular wires is due to relative mobility of the twin boundaries.

Due to the deformation via twinning, the fracture strain is larger in the rectangular ⟨100⟩/{100} nanowires. As can be seen in figure 4, the square wire breaks at a strain of around $\epsilon_f = 0.41$ and the rectangular 20 × 5 wire breaks at a strain of $\epsilon_f = 0.48$. The toughness, which is used to characterize the amount of absorbed energy density at the fracture point, is 0.94 GJ m^{-3} for the rectangular 20 × 5 wire and 1.69 GJ m^{-3} for the square 5 × 5 wire. The toughness of the square wire is larger despite the smaller fracture strain due to the larger yield stress, strain and post-yield stress plateau resulting from the higher-energy defects present in the wire.

The stress–strain curves of the ⟨100⟩/{110} wires are presented in figure 4(b). The square 5 × 5 wire yields at 12.6 GPa, while the rectangular 20 × 5 wire yields at 9 GPa. In the post-yield deformation, no propagation of stacking faults

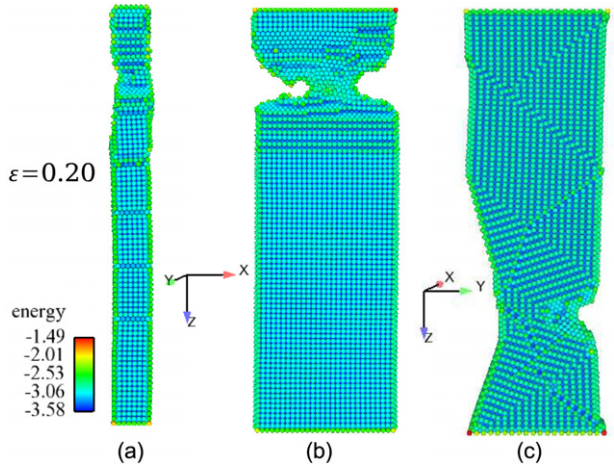

Figure 5. Snapshots of the tensile deformation of ⟨110⟩/{100}{110} nanowires at a strain of $\epsilon = 0.20$: (a) 5 × 5 CLU cross section; (b) 20 × 5 CLU cross section; (c) 5 × 20 CLU cross section. Potential energy is in units of eV.

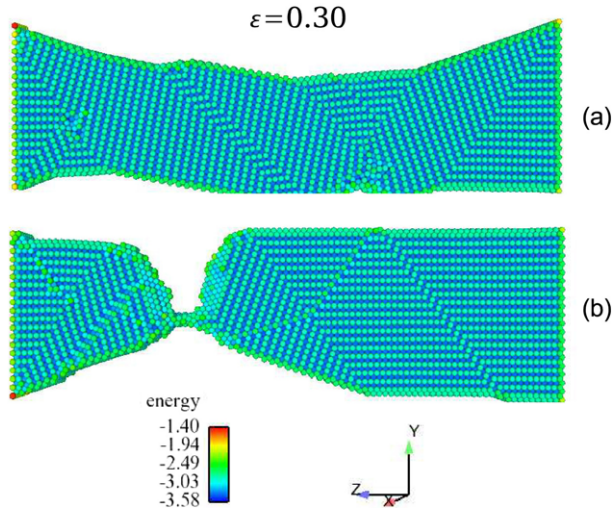

Figure 6. Snapshots of two tensile-loaded ⟨110⟩/{100}{110} nanowires with large {110} surfaces: (a) 4 × 20 CLU cross section; (b) 5 × 20 CLU cross section. Potential energy is in units of eV.

is observed and thus there is no obvious stress plateau in ⟨100⟩/{110} wire, leading to brittle fracture around $\epsilon_f = 0.30$ for both square and rectangular wires. Due to the brittle failure mode, the square ⟨100⟩/{110} wires have a smaller toughness of 1.12 GJ m^{-3} compared to the corresponding ⟨100⟩/{100} wires, while the rectangular ⟨100⟩/{110} wires, due to their elevated yield stress and strain, have a similar toughness of 0.92 GJ m^{-3} compared to the rectangular ⟨100⟩/{100} wires. A summary of the computed toughness for the ⟨100⟩/{100} and ⟨100⟩/{110} wires is given in table 3.

3.2. *Tension of* ⟨110⟩/{100}{110} *nanowires*

We now present our simulation results on the tensile-loaded ⟨110⟩ nanowires, including both ⟨110⟩/{100}{110} and ⟨110⟩/{111}{112} configurations. The dimensions of these nanowires are shown in table 2. Since each wire has two different surface orientations present, we consider two different rectangular configurations for each wire to illustrate the influence of each side surface orientation.

Representative snapshots of the inelastic deformation of three ⟨110⟩/{100}{110} nanowires are illustrated in figure 5. The rectangular nanowires depicted in figures 5(b) and (c) have cross-sectional dimensions of 20 × 5, and thus large {100} side surfaces, and 5 × 20, which has large {110} side surfaces. As is shown, the three wires exhibit distinct deformation modes at a strain of $\epsilon = 0.20$. The square nanowire with cross-sectional dimensions of 5 × 5 accommodates the plastic deformation through the slip of full and partial dislocations, resulting in distributed stacking faults along the wire length. Unlike the deformation seen in the square cross section ⟨100⟩ nanowires, these distributed stacking faults are immobile along the wire length, leading to localized necking in the post-yield deformation period and thus a small fracture strain.

The rectangular nanowire with large {100} side surfaces, 20 × 5, exhibits localized plastic deformation. As shown in figure 5(b), at a strain of $\epsilon = 0.20$, the wire has a perfect crystal structure everywhere except at regions of local deformation, resulting in a small fracture strain. By examining the deformation process, we have found that the stacking faults that nucleate from the {100} surfaces move and annihilate due to the surface crystallographic structure, resulting in a surface step or full dislocation on the {100} surfaces. This surface step decreases the ductility of the wire as it locally reduces the mobility of stacking faults due to partial dislocations; thus the low ductility of this rectangular wire is attributed to the side surface orientation.

The 5 × 20 rectangular wire with large {110} side surfaces exhibits a different deformation behaviour under tensile loading. As shown in figure 5(c), portions of the large {110} side surface rotate due to the tensile loading and form a new {110} facet on a different crystal variant. This newly formed {110} facet is separated from the initial facet by a twin boundary, as shown in figure 5(c). The rotation of the {110} surface causes a reorientation of the small {100} side surfaces to become {110} surfaces. Overall, due to the influence of the small {100} side surfaces, the twinning-dominated reorientation was interrupted by a localized fracture in the post-yield period, as shown in figure 5(c). To reduce the influence of {100} side surfaces further, we performed another simulation on a rectangular ⟨110⟩/{100}{110} nanowire with cross-sectional dimensions of 4 × 20, one layer thinner than the 5 × 20 nanowire. As shown in figure 6, the thin wire displayed a more organized twinning, leading to fracture strains far exceeding those observed in the other ⟨110⟩/{100}{110} nanowires. Thus the thickness reduction does have a great influence on the deformation modes of metal nanowires by minimizing the influence of the {100} surfaces.

The stress–strain curves of the ⟨110⟩/{100}{110} wires are presented in figure 7(a). As is shown, the rectangular 20 × 5 wire with large {100} surfaces has a high yield stress, 6.3 GPa, which is similar to that of the square nanowire, 6.0 GPa, while the 5 × 20 wire with large {110} surfaces exhibits a smaller yield stress, 4.1 GPa. The similar yield stresses of the square nanowire and the rectangular wires with large {100} surfaces

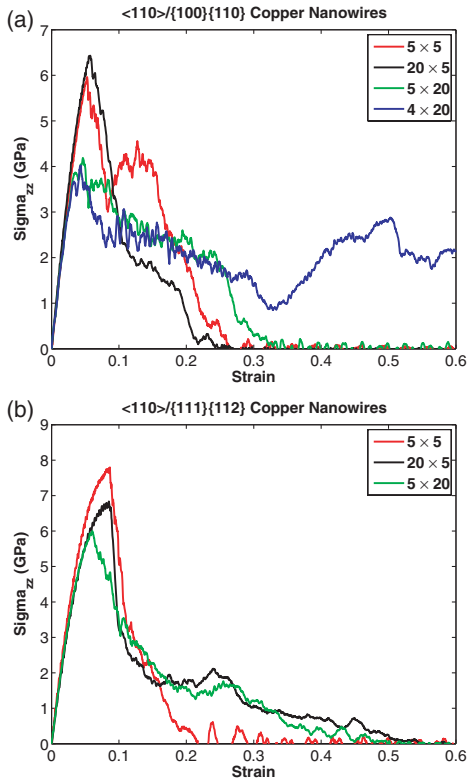

Figure 7. Stress–strain curves of tensile-loaded ⟨110⟩ copper nanowires: (a) ⟨110⟩/{100}{110} wires; (b) ⟨110⟩/{111}{112} wires.

Table 4. The toughness (μ_t) of ⟨110⟩ copper nanowires under tensile loading. The values are in units of GJ m^{-3} and correspond to the wires in table 2.

Orientation	1	2	3	4	5	6	7
⟨110⟩/{100}{110}	0.58	0.96	0.78	0.75	1.35	0.68	0.71
⟨110⟩/{112}{111}	0.94	0.81	0.76	0.72	0.68	0.80	0.87

can be attributed to the same yield mechanism, slip of higher-energy full and lower energy partial dislocations, and the small difference in relaxation strain along the ⟨110⟩ axial orientation. In contrast, the lower yield stress of the rectangular wires with large {110} surfaces is due to the twinning-dominated deformation, which is characterized by the nucleation and propagation of energetically favourable partial dislocations.

In the post-yield period of the ⟨110⟩/{100}{110} wires, the 5 × 5 and 20 × 5 wires exhibit a fracture strain of $\epsilon_f = 0.25$ due to the localized deformation, while the fracture strain of the 20 × 5 wire is around $\epsilon_f = 0.32$, where the increase in fracture strain is due to the twinning-dominated deformation, as shown in figure 5(c). The magnitude of fracture strain can be further improved by reducing the wire thickness, which minimizes the influence of the {100} surfaces. As shown in table 4, the toughness is low for the rectangular 20 × 5 wire due to the small fracture strain resulting from the localized deformation, while for the 5 × 20 wire, the high toughness is due to the large fracture strain resulting from the twinning deformation. In general, the toughness does not appear to vary greatly between square and rectangular geometries for ⟨110⟩/{100}{110} nanowires.

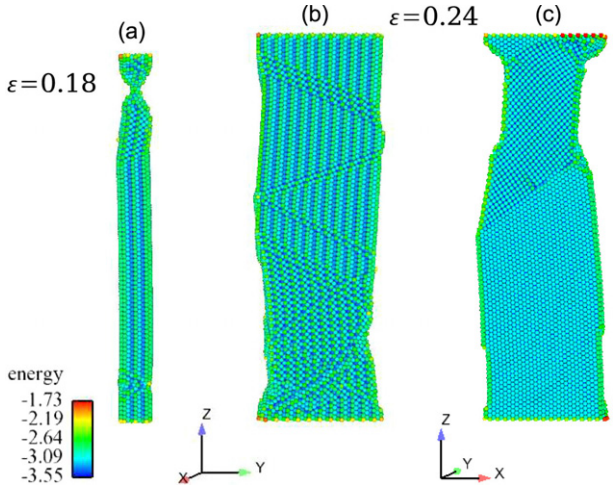

Figure 8. Snapshots of the tensile deformation of ⟨110⟩/{111}{112} nanowires: (a) 5 × 5 CLU cross section; (b) 20 × 5 CLU cross section; (c) 5 × 20 CLU cross section. Potential energy is in units of eV.

3.3. Tension of ⟨110⟩/{111}{112} *nanowires*

We now consider the inelastic deformation modes of the tensile-loaded ⟨110⟩/{111}{112} nanowires. Representative snapshots of these nanowires are displayed in figure 8. As is shown, these three nanowires exhibit three distinct inelastic deformation modes. The square nanowire deforms plastically by showing localized deformation, which leads to a small fracture strain. The rectangular 20 × 5 nanowire with large {112} side surfaces exhibits a loading-induced surface reorientation from {111} to {100} on the small side surfaces and {112} to a high index orientation on the large side surfaces, as shown in figure 8(b). The rectangular 5 × 20 nanowire with large {111} surfaces exhibits a surface reorientation with the {111} surfaces reorienting to {100} surfaces due to the tensile loading; a similar reorientation has been shown to lead to shape memory and pseudoelastic properties in rhombic ⟨110⟩/{111} nanowires [9, 10]. As shown in figure 8(c), at a strain of $\epsilon = 0.18$, the nanowire show a reoriented {100} facet, which is separated from the remaining {111} surface by a twin boundary layer. Thus the two rectangular ⟨110⟩/{111}{112} nanowires deform via twinning under tensile loading.

Stress–strain curves of ⟨110⟩/{111}{112} nanowires are presented in figure 7(b). As is shown, the square nanowire has a high yield stress, 7.8 GPa, followed by the rectangular 20 × 5 wire with large {112} surfaces, 6.8 GPa, and the 5 × 20 wire with a large {111} surface has the smallest yield stress, 6.0 GPa. The high yield stress in the square nanowire is related to the slip of energetically unfavourable full dislocations. More interestingly, the rectangular ⟨110⟩/{111}{112} nanowires have yield strengths that are similar to that of the square nanowire, as shown in figure 7(b). The reason for this is that the tensile-induced surface reorientation is from a lower-energy {111} surface to a higher-energy {100} surface; despite the low stress needed to nucleate and propagate the twin boundaries in those wires, the fact that the surface orientation changes from a low-energy and extremely stable {111} surface to a higher-energy {100} surface causes the rectangular ⟨110⟩/{111}{112}

nanowires to have yield stresses, 6.8 GPa, that are comparable to the yield value of the square ⟨110⟩/{111}{112} nanowire, 7.8 GPa.

In the post-yield period, the localized deformation behaviour in the square nanowire leads to a small fracture strain of about $\epsilon_f = 0.22$, while the two rectangular wires fracture at a strain of about $\epsilon_f = 0.45$ due to the twinning-dominated reorientation. The toughness of these nanowires is summarized in table 4, which shows that the toughness of the square nanowire is 0.72 GJ m^{-3}, while the toughness of the rectangular wires is much higher, 0.94 GJ m^{-3} for the rectangular ⟨110⟩ wire with large {112} surfaces, and 0.87 GJ m^{-3} for the rectangular ⟨110⟩ wire with large {111} surfaces. Again, the high toughness is due to the energetically unfavourable reorientation of low-energy {111} surfaces to {100} surfaces in conjunction with the ductile failure due to the nucleation and propagation of mobile twin boundaries.

4. Conclusions

In conclusion, we have utilized atomistic simulations in conjunction with an embedded atom potential to analyse the coupled effects of cross-sectional geometry and side surface orientation on the inelastic deformation mechanisms and resulting mechanical properties of copper nanowires. The overarching theme of this work was to quantify the link between the observed deformation mechanisms due to non-square cross-sectional geometries and the observed mechanical properties under tensile loading, and also to illustrate that geometry can be utilized to tailor the mechanical properties of nanowires.

The specific findings can be summarized as follows. (1) Non-square nanowires generally exhibit lower yield stresses and strains, lower fracture toughness, elevated fracture strains and a propensity to deform via twinning. (2) The lower yield stresses and strains of rectangular nanowires generally arise due to the fact that they deform via twinning, which is due to the nucleation and propagation of mobile partial dislocations. In contrast, square nanowires tend to deform via both energetically favourable partial dislocations and energetically unfavourable full dislocations, which increases their yield properties. (3) Rectangular wires that undergo a tensile-induced surface reorientation from a lower-energy ({111}) to higher-energy ({100}) surface tend to have yield properties that are comparable to the corresponding square wires; this occurs due to the work necessary to convert the stable, low-energy surfaces to less stable and thus higher-energy surfaces. Furthermore, the surface reorientation in conjunction with the mobile propagating twin boundaries leads to those rectangular wires having fracture toughnesses and fracture strains that exceed those seen in the square nanowires.

The current results indicate that nanowires of other crystalline structures, for example silicon wires which have a diamond structure or zinc oxide nanowires which may form in multiple crystal structures, are likely to exhibit similar variance in mechanical behaviour and properties through alteration of geometry and surface orientation. This fact may be useful in performing future nanoscale experiments, including those investigating mechanical properties only, but also in studying coupled physics phenomena such as optomechanics [16] and piezoresistivity [64]; it is likely that these properties, which are of critical interest in NEMS, may be strongly impacted by the geometry and surface orientations of the nanowires.

Acknowledgment

The authors gratefully acknowledge funding from the Vanderbilt University Discovery Grant in support of this research.

References

[1] Lieber C M 2003 Nanoscale science and technology: building a big future from small things *MRS Bull.* **28** 486–91
[2] Patolsky F, Zheng G and Lieber C M 2006 Nanowire sensor for medicine and the life science *Nanomedicine* **1** 51–65
[3] Vivekchand S R C, Ramamurty U and Rao C N R 2006 Mechanical properties of inorganic nanowire reinforced polymermatrix composites *Nanotechnology* **17** S344–50
[4] Xia Y, Yang P, Sun Y, Wu Y, Mayers B, Gates B, Yin Y, Kim F and Yan H 2003 One-dimensional nanostructures: synthesis, characterization, and applications *Adv. Mater.* **15** 353–89
[5] Lieber C M and Wang Z L 2007 Functional nanowires *MRS Bull.* **32** 99–104
[6] Craighead H G 2000 Nanoelectromechanical systems *Science* **290** 1532–5
[7] Ekinci K L and Roukes M L 2005 Nanoelectromechanical systems *Rev. Sci. Instrum.* **76** 061101
[8] Diao J, Gall K and Dunn M L 2003 Surface-stress-induced phase transformation in metal nanowires *Nat. Mater.* **2** 656–60
[9] Park H S, Gall K and Zimmerman J A 2005 Shape memory and pseudoelasticity in metal nanowires *Phys. Rev. Lett.* **95** 255504
[10] Liang W, Zhou M and Ke F 2005 Shape memory effect in Cu nanowires *Nano Lett.* **5** 2039–43
[11] Zhou L G and Huang H 2004 Are surfaces elastically softer or stiffer? *Appl. Phys. Lett.* **84** 1940–2
[12] Cammarata R C 1994 Surface and interface stress effects in thin films *Prog. Surf. Sci.* **46** 1–38
[13] Wiley B J, Wang Z, Wei J, Yin Y, Cobden D H and Xia Y 2006 Synthesis and electrical characterization of silver nanobeams *Nano Lett.* **6** 2273–8
[14] Rubio G, Agrait N and Vieira S 1996 Atomic-sized metallic contacts: mechanical properties and electronic transport *Phys. Rev. Lett.* **76** 2302–5
[15] Ohnishi H, Kondo Y and Takayanagi K 1998 Quantized conductance through individual rows of suspended gold atoms *Nature* **395** 780–3
[16] Lyons D M, Ryan K M, Morris M A and Holmes J D 2002 Tailoring the optical properties of silicon nanowire arrays through strain *Nano Lett.* **2** 811–6
[17] Audoit G, Mhuircheartaigh E N, Lipson S M, Morris M A, Blau W J and Holmes J D 2005 Strain induced photoluminescence from silicon and germanium nanowire arrays *J. Mater. Chem.* **15** 4809–15
[18] Buda F, Kohanoff J and Parrinello M 1992 Optical properties of porous silicon: a first-principles study *Phys. Rev. Lett.* **69** 1272–5
[19] Brus L E, Szajowski P F, Wilson W L, Harris T D, Schuppler S and Citrin P H 1995 Electronic spectroscopy and photophysics of Si nanocrystals: relationship to bulk c-Si and porous Si *J. Am. Chem. Soc.* **117** 2915–22
[20] Wu B, Heidelberg A and Boland J J 2005 Mechanical properties of ultrahigh-strength gold nanowires *Nat. Mater.* **4** 525–9
[21] Tabib-Azar M, Nassirou M, Wang R, Sharma S, Kamins T I, Islam M S and Williams R S 2005 Mechanical properties of self-welded silicon nanobridges *Appl. Phys. Lett.* **87** 113102

[22] Heidelberg A, Ngo L T, Wu B, Phillips M A, Sharma S, Kamins T I, Sader J E and Boland J J 2006 A generalized description of the elastic properties of nanowires *Nano Lett.* **6** 1101–6

[23] Silva E C C M, Tong L, Yip S and Van Vliet K J 2006 Size effects on the stiffness of silica nanowires *Small* **2** 239–43

[24] Wong E W, Sheehan P E and Lieber C M 1997 Nanobeam mechanics: elasticity, strength, and toughness of nanorods and nanotubes *Science* **277** 1971–5

[25] Cuenot S, Frétigny C, Demoustier-Champagne S and Nysten B 2004 Surface tension effect on the mechanical properties of nanomaterials measured by atomic force microscopy *Phys. Rev.* B **69** 165410

[26] Rodrigues V, Fuhrer T and Ugarte D 2000 Signature of atomic structure in the quantum conductance of gold nanowires *Phys. Rev. Lett.* **85** 4124–7

[27] Kizuka T, Takatani Y, Asaka K and Yoshizaki R 2005 Measurements of the atomistic mechanics of single crystalline silicon wires of nanometer width *Phys. Rev.* B **72** 035333

[28] Jing G Y, Duan H L, Sun X M, Zhang Z S, Xu J, Li Y D, Wang J X and Yu D P 2006 Surface effects on elastic properties of silver nanowires: contact atomic-force microscopy *Phys. Rev.* B **73** 235409

[29] Landman U, Luedtke W D, Burnham N A and Colton R J 1990 Atomistic mechanisms and dynamics of adhesion, nanoindentation, and fracture *Science* **248** 454–61

[30] Branicio P S and Rino J P 2000 Large deformation and amorphization or Ni nanowires under uniaxial strain: a molecular dynamics study *Phys. Rev.* B **62** 16950–5

[31] Kang J-W and Hwang H-J 2001 Mechanical deformation study of copper nanowires using atomistic simulation *Nanotechnology* **12** 295–300

[32] Wu H A, Soh A K, Wang X X and Sun Z H 2004 Strength and fracture of single crystal metal nanowire *Key Eng. Mater.* **261–263** 33–8

[33] Liang W and Zhou M 2004 Response of copper nanowires in dynamic tensile deformation *Proc. Inst. Mech. Eng.* C **218** 599–606

[34] Sanchez-Portal D, Artacho E, Junquera J, Ordejon P, Garcia A and Soler J M 1999 Stiff monatomic gold wires with a spinning zigzag geometry *Phys. Rev. Lett.* **83** 3884–7

[35] da Silva E Z, da Silva A J R and Fazzio A 2001 How do gold nanowires break? *Phys. Rev. Lett.* **87** 256102

[36] Park H S and Zimmerman J A 2005 Modeling inelasticity and failure in gold nanowires *Phys. Rev.* B **72** 054106

[37] Mehrez H and Ciraci S 1997 Yielding and fracture mechanisms of nanowires *Phys. Rev.* B **56** 12632–42

[38] Gall K, Diao J and Dunn M L 2004 The strength of gold nanowires *Nano Lett.* **4** 2431–6

[39] Coura P Z, Legoas S G, Moreira A S, Sato F, Rodrigues V, Dantas S O, Ugarte D and Galvao D S 2004 On the structural and stability features of linear atomic suspended chains formed from gold nanowires stretching *Nano Lett.* **4** 1187–91

[40] Park H S, Gall K and Zimmerman J A 2006 Deformation of FCC nanowires by twinning and slip *J. Mech. Phys. Solids* **54** 1862–81

[41] Ji C and Park H S 2007 Characterizing the elasticity of hollow metal nanowires *Nanotechnology* **18** 115707

[42] Koh A S J and Lee H P 2006 Shock-induced localized amorphization in metallic nanorods with strain-rate-dependent characteristics *Nano Lett.* **6** 2260–7

[43] Leach A M, McDowell M and Gall K 2007 Deformation of top-down and bottom-up silver nanowires *Adv. Funct. Mater.* **17** 43–53

[44] Park H S 2006 Stress-induced martensitic phase transformation in intermetallic nickel aluminum nanowires *Nano Lett.* **6** 958–62

[45] Fang X and Zhang L 2006 Controlled growth of one-dimensional oxide nanomaterials *J. Mater. Sci. Technol.* **22** 1–18

[46] Fang X, Ye C, Zhang L, Wang Y and Wu Y 2005 Temperature-controlled catalytic growth of ZnS nanostructures by evaporation of ZnS nanopowders *Adv. Funct. Mater.* **15** 63–8

[47] Kelly K L, Coronado E, Zhao L L and Schatz G C 2003 The optical properties of metal nanoparticles: the influence of size, shape, and dielectric environment *J. Phys. Chem.* B **107** 668–77

[48] Sun Y and Xia Y 2003 Alloying and dealloying processes involved in the preparation of metal nanoshells through a galvanic replacement reaction *Nano Lett.* **3** 1569–72

[49] Wiley B, Sun Y, Mayers B and Xia Y 2005 Shape-controlled synthesis of metal nanostructures: the case of silver *Chem. Eur. J.* **11** 454–63

[50] Ji C and Park H S 2006 Geometric effects on the inelastic deformation of metal nanowires *Appl. Phys. Lett.* **89** 181916

[51] Daw M S and Baskes M I 1984 Embedded-atom method: Derivation and application to impurities, surfaces, and other defects in metals *Phys. Rev.* B **29** 6443–53

[52] Daw M S, Foiles S M and Baskes M I 1993 The embedded-atom method: a review of theory and applications *Mater. Sci. Rep.* **9** 251–310

[53] Mishin Y, Mehl M J, Papaconstantopoulos D A, Voter A F and Kress J D 2001 Structural stability and lattice defects in copper: *ab initio*, tight-binding, and embedded-atom calculations *Phys. Rev.* B **63** 224106

[54] Kondo Y and Takayanagi K 1997 Gold nanobridge stabilized by surface structure *Phys. Rev. Lett.* **79** 3455–8

[55] Wang Z L, Gao R P, Nikoobakht B and El-Sayed M A 2000 Surface reconstruction of the unstable {110} surface in gold nanorods *J. Phys. Chem.* B **104** 5417–20

[56] Nosé S 1984 A unified formulation of the constant temperature molecular dynamics methods *J. Chem. Phys.* **81** 511–9

[57] Hoover W G 1985 Canonical dynamics: equilibrium phase-space distributions *Phys. Rev.* A **31** 1695–7

[58] Plimpton S J 1995 Fast parallel algorithms for short-range molecular dynamics *J. Comput. Phys.* **117** 1–19

[59] Warp 2006 http://www.cs.sandia.gov/~sjplimp/lammps.html

[60] Zhou M 2003 A new look at the atomic level virial stress: on continuum-molecular equivalence *Proc. R. Soc.* A **459** 2347–92

[61] Zimmerman J A, Webb E B III, Hoyt J J, Jones R E, Klein P A and Bammann D J 2004 Calculation of stress in atomistic simulation *Modelling Simul. Mater. Sci. Eng.* **12** S319–32

[62] Kelchner C L, Plimpton S J and Hamilton J C 1998 Dislocation nucleation and defect structure during surface indentation *Phys. Rev.* B **58** 11085–8

[63] Park H S and Klein P A 2007 Surface Cauchy–born analysis of surface stress effects on metallic nanowires *Phys. Rev.* B **75** 085408

[64] He R and Yang P 2006 Giant piezoresistive effect in silicon nanowires *Nat. Nanotechnol.* **1** 42–6